

Multiphase dolomitization in Devonian Shogram Formation, Chitral, Karakorum ranges, Pakistan: Evidence from outcrop analogue, petrography, and geochemistry

Maryam Saleem^{a,b}, Faisal Rehman^a, Emad U. Khan^a, Syed W. Sajjad^a, Tahir Azeem^a, Asad Jadoon^a, Abbas A. Naseem^{a,*}

^a Department of Earth Sciences, Quaid-e-Azam University, Islamabad 45320 Pakistan

^b Department of Earth & Environmental Sciences, Bahria University, Islamabad 44000 Pakistan

*Corresponding author, e-mail: abbasaliqau@gmail.com

Received 5 Jul 2021, Accepted 25 Nov 2021

Available online 28 Feb 2022

ABSTRACT: This paper reports the first detailed microscopic and geochemical investigations of multiphase dolomitization in Devonian Shogram Formation, North-Western Karakorum constraining nature and origin of dolomitizing fluids. Field and petrographic studies revealed 4 different types of replacive dolomites, which are (i) fine grained anhedral dolomite (D1), (ii) medium grained subhedral to anhedral dolomite (D2), (iii) medium grained euhedral dolomite (D3), and (iv) coarse grained anhedral dolomite (D4) along with cement phase saddle dolomite (SD). These dolomites had high Fe and Mn concentrations and low Sr content. Stable isotope studies indicated high light isotope $\delta^{18}\text{O}$ values for D1 and D2, higher lighter isotope $\delta^{18}\text{O}$ value for D3, and highest lightest isotope $\delta^{18}\text{O}$ values for D4 and SD, respectively. Petrographical and geochemical data suggested that D1 and D2 are likely formed in compactional flow regime in early stages prior to chemical compaction at shallow burial depths, whereas D3 is formed in late diagenetic deep burial settings. Lastly, D4 and SD are formed from high temperature hydrothermal fluids. These fluids could be related to widespread tectonic activity in the Karakorum region during collision or post-collisional time. Reshun fault acted as an important pathway that channeled Mg-rich hydrothermal fluids from underlying strata into carbonates, which caused intense dolomitization.

KEYWORDS: dolomitization, Karakorum, saddle dolomite

INTRODUCTION

The dolomite is the unique carbonate rock that forms from the process of dolomitization. The fluid-driving mechanisms, variation in temperature, and different chemical compositions of the dolomitizing fluids can be revealed by petrography, geochemistry, isotopic signatures, and their spatial distribution [1].

In recent years, hydrothermal processes are considered an important mechanism for massive dolomites formation. Hydrothermal dolomitization has become important because of the extensive distribution of deep-burial dolomites containing oil, natural gas resources, and ore deposits [2]. Deep seated faults and fractures act as pathways which channel episodic flow of basinal fluids [3].

Numerous researchers worked on different characteristics of dolomite bodies, particularly specifying the fluid flow mechanism causing dolomitization [4]. Most of the dolomite in geologic record is formed by replacement of calcite. Fluid-driving mechanism and Mg source for dolomites in Devonian Shogram Formation, Chitral, Pakistan has not been reported yet, and no work has been carried out till now. In this study, detailed field investigations, petrographic studies, and geochemical analysis (elemental and isotope analysis) have been used to evaluate the characteristics and diagenetic history of dolomites of Shogram Formation.

GEOLOGICAL SETTING

The Karakoram block is a belt of high mountain terrain which resulted from a rapid uplift of a thickened continental crust (55–70 km) during the Pliocene [5]. This uplifting is in the response to the Indian-Eurasian continental collision [5]. The Karakorum block is the southern part of the Eurasian side of collision zone, and geologically it can be related to Central Tibet Qiantang terrain [6]. Repeated collisions of continental blocks and plates from Jurassic to Present make Karakorum range a very complex one [7]. Central eastern part of the North Karakoram terrain consists of strongly deformed Permo-Mesozoic sedimentary succession, which escaped strong metamorphism during India-Eurasia collision [8]. Numerous thrust sheets are present in North Karakorum, exhibiting complex geometrical relationship. To the northwest, it contains alkali basalts, tuffs, and dolostones of Tash Kupruk Zone (TKZ) which are bounded by shear faults [9]. At least 3 thrust sheets south of TKZ contain Devonian rocks, which are Siru Gol, Lashkargaz/Baroghil, and Karamber thrust sheets [10, 11]. Southwards, Reshun Fault (RF) is present, which joins the Upper Hunza Fault in the east and extends for more than 200 km area [11]. In the sedimentary belt of NW Karakorum, Devonian rocks are present in numerous thrust sheets, both to the south and to the north of RF [7]. The

Late Cretaceous Reshun Formation is present on the footwall of Reshun Fault, which unconformably covers Jurassic and Cretaceous rocks. Westwards, Devonian rocks are present on the hanging wall of RF [12]. The massive crinoidal dolomite was overlain by bedded dolomite and massive cross-bedded fine to medium grained quartzite at the top [7]. Tabulate rugosan and brachiopod species were identified in Shogram Formation, which are of Middle Devonian age [12].

Study area lies in Chitral near Shogram mount, Northwestern Karakorum (Fig. S1a). It is a part of northern sedimentary belt of the Karakorum block which continue westwards into Baroghil and beyond [7]. In Chitral, it is limited only to narrow belt and consists of Paleozoic to Mesozoic sequence (Fig. S1b).

MATERIALS AND METHODS

Excellent exposure of Devonian Shogram Formation is present at Shogram Mount section near Reshun village. Detailed field investigation of the dolomites of Shogram Formation in the study area was carried out, which helped in identifying several dolomite and calcite phases. Overall, 139 samples of dolomites and various diagenetic features were collected in the study area. The 114 thin sections were prepared at Hydrocarbon Development Institute of Pakistan and were stained with Alizarin Red S and K-ferricyanide solution [13] to differentiate between dolomite and calcite and carefully examined for petrographic observation using conventional microscopy (Olympus CX31 along with DP-21 camera attachment) at Department of Earth Sciences Quaid-e-Azam University Islamabad, Pakistan. Inductively coupled plasma-optical emission spectrometry (ICP-OES) technique was used to determine major and trace element composition, which was carried out on 41 samples at Pakistan Institute of Nuclear Sciences and Technology (PINSTECH). For ICP-OES analysis, digestions of rock powder sample were carried out where 100 mg of each powder sample were weighed through a digital balance, followed by the addition of 9.0 ml of Aqua Regia and were left at room temperature overnight. After that, the samples were heated in a closed vessel microwave for 3 steps: at 120 °C for 10 min, followed by 220 °C for 20 min, and finally heating again for 5 min at 220 °C. After digestion, the samples were filtered, then diluted with 50.0 ml distilled-deionized water and filtered again. This procedure was performed in triplicate. Through ICP-OES method, 70 elements having atomic number up to 83 together with Th and U can be measured instantaneously. The elements like sodium (Na), strontium (Sr), manganese (Mn), and iron (Fe) are particularly striking in terms of determination of diagenetic process, nature of dolomitizing fluids as well as deduction of the dolomitization model. Stable oxygen and carbon isotope analyses on 22 selected

samples of different dolomite and calcite phases were carried out at Isotope Application Division, PINSTECH, Islamabad. All stable isotope values were reported in per mill (‰) relative to Vienna Pee Dee Belemnite (V-PDB). Fractionation factors were used to correct dolomite isotopic composition given by Rosenbaum and Sheppard [14].

RESULTS

Field Observations

Total thickness of Devonian Shogram Formation in Shogram Mount section is 800 m [15] which is thrust over Cretaceous Reshun Formation (Fig. 1a). Lithologically, Shogram Formation consists of dolomite, limestone, quartzite, and intercalated shale. Since this paper targets only the dolomitic portion of Shogram Formation, only dolomitic units are discussed here in detail. In the study area, excellent outcrop of Shogram Formation consisted of alternating beds of thick and thin bedded dolomite units (Fig. 1b-c); limestone was fossiliferous and contained different types of bioclasts (Fig. 1d). Moreover, at places ossicles were also found in dolomites (Fig. 1e). The dolomites in the study area were identified based on color contrast and elephant skin weathering (Fig. 1f-g). In addition, yellowish white colored saddle dolomite (SD) cement phase mostly occurred as vein- and vug-filling (Fig. 1h-i). Furthermore, multiple episodes of calcite cementation occurred in form of vein and postdated earlier formed dolomites (Fig. 1j). Mechanical and chemical compaction was also observed in the form of fracture and stylolites (Fig. 1k). Pyrite was also observed in the form of vein- and vug-filling in earlier formed dolomites (Fig. 1l).

Petrography

Thin section of precursor limestone exhibited distinct depositional features which include peloids, intra-clasts, and bioclasts (Fig. 2a). Conventional microscopic examination was used to identify and differentiate different dolomite phases based on crystal shape and size by using the classification scheme by Sibley and Gregg [16]. Four replacive dolomitic phases and one cement phase SD were recognized in Shogram Formation. Replacive dolomite phases included: (i) fine grained anhedral dolomite (D1), (ii) medium grained subhedral to anhedral dolomite (D2), (iii) medium grained euhedral dolomite (D3), and (iv) coarse grained anhedral dolomite (D4). Other diagenetic alterations included blocky calcite and twinned calcite cementation. D1 was thin bedded light grey color and exhibited non-planar interlocking anhedral crystal morphology with size ranging from 20 μm to 40 μm which had fractures filled by later stage pyrite (Fig. 2b). The dolomite D1 has obliterated the original fabric of the precursor rock although at places, partial dolomitization of peloids was also observed (Fig. 2c).

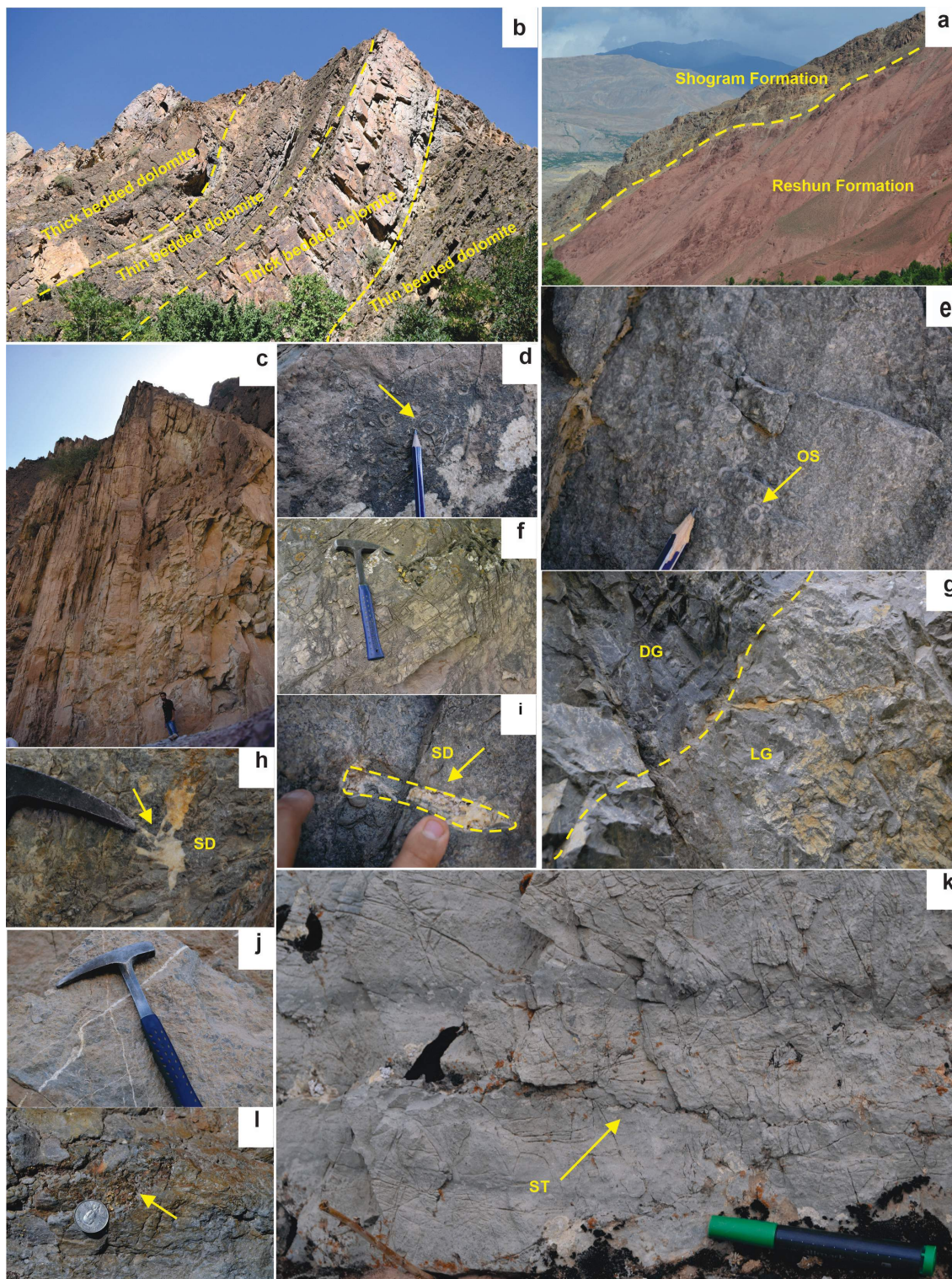


Fig. 1 Field photographs. (a) Faulted contact between Shogram Formation and Reshun Formation. (b) Panoramic view of the study area showing thick and thin bedded dolomite. (c) Vertically dipping thin bedded dolomites of Shogram Formation. (d) Arrow indicating the bioclasts in limestone of Shogram Formation. (e) Ossicles (OS) indicated by arrow in the dolomite unit. (f) Elephant skin weathering in dolomite. (g) Contact between light gray (LG) and dark grey (DG) dolomites. (h) Dolomite clasts floating in pore filling SD shown with an arrow. (i) SD represented by arrow in the form of patches. (j) Multiple sets of calcite veins cross cutting each other. (k) Arrow showing low to high amplitude stylolites. (l) Pyrite mineralization as indicated by arrow. Please see meaning of abbreviations in the abstract.

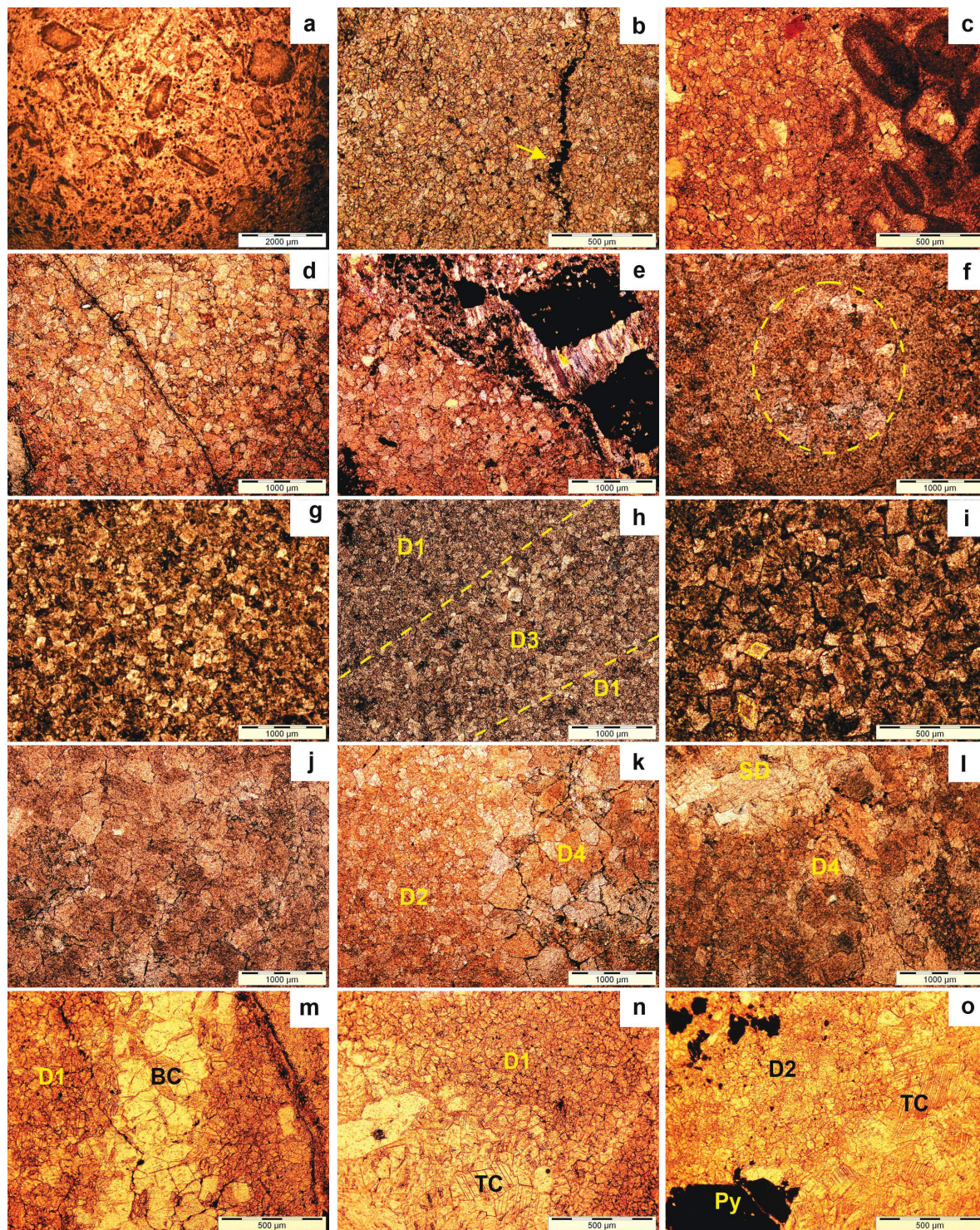


Fig. 2 Photomicrographs. (a) Bioclastic limestone. (b) D1 interlocked with each other along with fractures filled pyrite shown with an arrow. (c) D1 replacing peloids. (d) D2 having fractures. (e) Pyrite mineralization along with quartz. (f) Partially dolomitized ossicles. (g) D3 interlocked with each other and having cloudy rims. (h) Dolomite D3 crosscutting earlier formed D1. (i) Zonation in dolomite D3. (j) Coarse grained anhedral dolomite (D4). (k) Contact between dolomite D4 and D2. (l) Contact between SD and dolomite D4. (m) Granular blocky calcite cement (BC) crosscutting fine grained dolomite D1. (n) Contact between twinned calcite (TC) and D1. (o) Twinned calcite cementation (TC) crosscutting dolomite D2 and predating pyrite mineralization. Please see meaning of abbreviations in the abstract.

Dolomite D2 was thick bedded, dark grey colored and exhibited crystal size ranging from 80 to 230 μm and displayed non-planar subhedral to anhedral crystal texture with irregular crystal boundaries (Fig. 2d). The fabric destructive fractures of dolomite D2 were filled by pyrite while at some places, pyrite also occurred in disseminated form (Fig. 2e). Partial dolomitization of ossicles was also noticeable in D2 (Fig. 2f). Dolomite D3 was the third stage of dolomitization having crystal size ranging from 200–300 μm . This dolomite commonly exhibited homogenous to weak undulatory extinction. D3 was abundant, fabric destructive having cloudy crystal appearance and had strongly destroyed the original depositional and earlier diagenetic features (Fig. 2g). Crystals of D3 crossed cut the earlier formed fine grained anhedral dolomite (Fig. 2h). The dolomite D3 crystal showed zoning (Fig. 2i). Dolomite D4 showed the presence of coarse crystalline non-planar tightly packed anhedral crystal texture with a crystal size ranging from 200 to 620 μm (Fig. 2j). It had sharp contact with D2 and exhibited small scale fractures (Fig. 2k). Saddle dolomite (SD) occurred as a fracture- and pore-filling cementing phase. It had planar subhedral crystal texture and ranged in size from 400 μm to 1 mm (Fig. 2l). Different phases of calcite cementation were also present which were mostly fracture-filling (Fig. 2m) and twinned as well as pore-filling (Fig. 2n). Pyrite mineralization also occurred in fractures and disseminated form (Fig. 2o).

Geochemistry

Major and trace element compositions

The determination of major and trace element compositions is important in understanding diagenetic process, dolomite origin (early or late) and helps in inferring dolomitization model. Identification of the following elements helps in detecting dolomitizing fluid: calcium, magnesium, sodium, strontium, manganese, and iron [17, 18]. For this purpose, ICP-OES analysis was carried out to determine the exact chemical compositions of the dolomites (Fig. 3). D1 contained an average of 4918.25 ppm of Fe, 155 ppm of Sr, and 412.41 ppm of Mn concentrations. D2 had an average of 8142.97 ppm of Fe concentration which exceeded the concentration in D1. In D3, the average concentration of Fe content was 9217.7 ppm. However, the average concentrations of Sr and Mn in D3 were 84.3 and 474.6 ppm, respectively. The average concentration of Fe in dolomite D4 was 10 056.75 ppm whereas the concentrations of Sr and Mn were 105 and 496.33 ppm, respectively.

Oxygen and carbon isotope

The oxygen isotope data reported by various authors showed a large variance with $\delta^{18}\text{O}$ values ranging from -3.8% to -4.2% and $\delta^{13}\text{C}$ values from 0% to 1.9% for Devonian seawater signatures considering starting

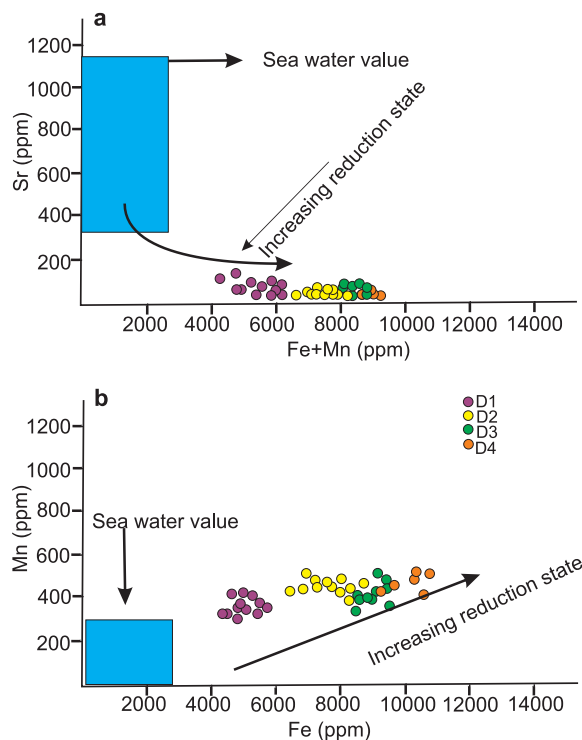


Fig. 3 Major and trace element cross-plots. (a) Sr and Fe+Mn concentrations of different dolomite phases along with sea water values. (b) Enrichment of Fe and Mn concentrations in different dolomite phases compared to seawater.

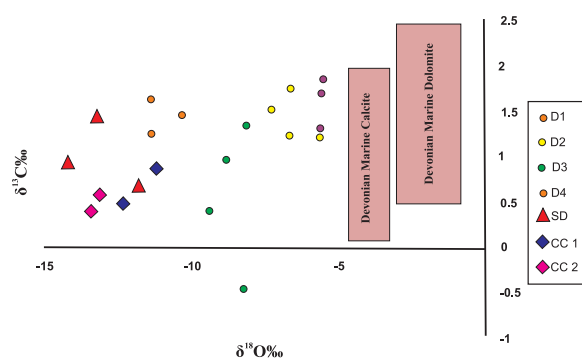


Fig. 4 Cross-plot between $\delta^{18}\text{O}$ and $\delta^{13}\text{C}$ values of the dolomites of Devonian Shogrom Formation compared with the expected Devonian marine calcite and dolomite.

values of the host limestone prior to interaction with magnesium-rich fluids, and values of Devonian marine dolomite $\delta^{13}\text{C}$ ranged from 0.5% to 2.5% and those of $\delta^{18}\text{O}$ ranged from -2.5% to -0.5% [19]. The oxygen and carbon compositions of the Shogrom Formation dolostone were given in Fig. 4. In the study area, different phases of dolomite revealed a wide range of isotopic signatures. The stable oxygen isotopic signatures $\delta^{18}\text{O}$ of D1 ranged from -5.245 to

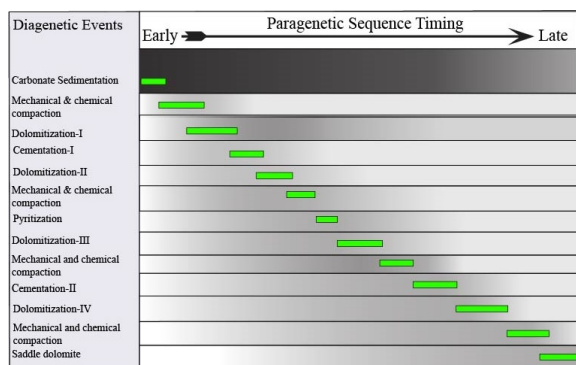


Fig. 5 Proposed paragenetic sequence of Devonian Shogrom Formation.

–6.025% V-PDB, and those of $\delta^{13}\text{C}$ ranged from +1.28 to +2.04% V-PDB. D2 showed comparatively more depleted values than D1, whereas D3 revealed the higher depleted $\delta^{18}\text{O}$ values which were –7.87 to –9.04% V-PDB and slightly depleted $\delta^{13}\text{C}$ signatures ranging from –0.49 to +1.36% V-PDB. D4 dolomite showed the highly depleted $\delta^{18}\text{O}$ signatures varying from –10.25 to –11.34% V-PDB and $\delta^{13}\text{C}$ signatures ranging from 1.28–1.71% V-PDB. Moreover, SD had the highest depleted $\delta^{18}\text{O}$ values ranging from –14.24 to –11.83% V-PDB; however, $\delta^{13}\text{C}$ values lied within the range of marine signatures which were +0.675 to +1.44% V-PDB. Additionally, CC1 displayed $\delta^{18}\text{O}$ values ranging from –11.24 to –12.34% V-PDB, whereas $\delta^{13}\text{C}$ values ranged from 0.48 to 0.87% V-PDB. Similarly, CC2 displayed even more depleted $\delta^{18}\text{O}$ signatures ranging from –13.15 to –13.43% V-PDB and $\delta^{13}\text{C}$ signatures ranging from 0.39 to 0.57% V-PDB.

DISCUSSION

The Karakorum block has recorded various stages of extensional and compressional tectonics during Paleozoic and Mesozoic such as Gondwana rifting, Kohistan-Karakorum collision, and associated plutonism [8, 20]. However, during Cenozoic, 4 major deformation events were reported [21]. The Paleocene to Eocene deformations was related to granitic magmatic intrusions, metamorphism, and crustal thickening, followed by Indian-Eurasian collision in Eocene. The southward motion along Main Karakorum Thrust (MKT) has been active since the closure of Indus Suture and up to Miocene and after [8]. Dextral motion is also observed along MKT in association with reverse faulting [8]. Moreover, tectonostratigraphic framework showed that Devonian shallow water carbonate platform deposits have undergone burial from Cretaceous (Kohistan-Karakorum collision) to Eocene (Karakorum-India Collision) to Miocene (Major Karakorum uplift) [8].

A detailed paragenetic sequence was established

on the basis of field observation and petrographic analyses of the Shogrom Formation (Fig. 5). After the deposition of Shogrom Formation in Devonian age, multiple phases of dolomitization have occurred, which involves the first phase of dolomitization, where peloidal structure is replaced by D1 (Fig. 2c). Fine grained dolomite indicated that less time and space was available for its formation and precipitation as compared to coarse grained dolomite. Moreover, D2 dolomite showed coarser crystal size but similar texture compared to D1. Dolomite crystal coarsening occurs because of slow precipitation rate [22], increase of temperature, and overgrowth of later stage dolomite on existent cores of earlier formed dolomite [23]. As compare to D1, the dolomite D2 reveals an increase in crystal size with clear crystal boundaries, slight increase in Fe and Mn concentrations and more negative trend of $\delta^{18}\text{O}$ from postulated values of Devonian marine dolomites. Evidence of meteoric diagenesis was absent in the Devonian Shogrom Formation. The depth of stylolitization in dolomites is considered fairly higher than that in limestones since dolomites are more resistant to dissolution [24]. D3 dolomite crystals had typically cloudy centers and clear rims (Fig. 2g,i). The cloudy center often represents post-depositional replacive dolomite or a precursor carbonate [25, 26]. D3 could form from direct replacement of carbonate or recrystallization of D1 and D2 [26]. Undulose extinction in D4 provided evidence of distorted crystal lattice caused by crystal growth at high temperatures (>60 °C) during deep burial settings [26, 27]. The occurrence of pyrite crystals as pore-filling as well in disseminated form suggested sulphide fluids circulated in the dolomitization process (Fig. 11, Fig. 3e). SD cement generation was limited to vugs filling and late fractures that cut through all earlier dolomite phases, which implies formation at the deepest diagenetic settings during progressive burial [26]. Hence, SD was formed after the replacive dolomites and following the brittle fracturing. Calcite cementation took place after the activation and reactivation of faults at different times which caused intense fracturing in dolomites. Likewise, post dolomite calcite cementation resulted in coarse twinned calcite cementation (Fig. 2n-o).

The Fe, Mn, Sr, and Na concentrations are usually used to identify process of diagenesis and the property of fluids [28]. Carbonate diagenesis leads to the increase in Mn and the decrease in Sr as shown in plenty of previous studies on the alteration extent using the Mn and Sr values [29]. The low concentrations of Sr (50–100 ppm) for all dolomite samples were comparable to those of ancient dolomite precipitated from marine waters (Fig. 2a-b) [30]. However, all dolomites showed evidence of decrease of Sr concentrations with increasing crystal size [31]. The high content of Fe and Mn in D3 and D4 could be associated to their formation under reducing conditions as compared to

D1 and D2 [32], or the high amount of Fe and Mn could be due to slow precipitation from higher temperature fluids [33].

Stable isotope analyses of dolomites showed depleted $\delta^{18}\text{O}$ values as compared to the original marine signatures of calcite and dolomite (Fig. 4). The first phase of replacive dolomite (D1) represented relatively less depleted $\delta^{18}\text{O}$ signatures as compared to D2, suggesting that D2 may have been formed at relatively high temperature. Similarly, D3 had more depleted values as compared to D1 and D2. The dolomite D4 had the highest depleted values of all the replacive dolomites (Fig. 4). Furthermore, dolomite (SD) and calcite (CC-I and CC-II) cements also exhibited highly depleted $\delta^{18}\text{O}$ values. More depleted oxygen isotopic trend of dolomite cement SD (-14.24 to -11.83% V-PDB) suggested that the fluids were originated from greater depths with higher temperatures than the replacive dolomitizing fluids. All the observed diagenetic phases showed deviation toward negative oxygen-isotopic signatures, and increased temperature was the likely source of depleted $\delta^{18}\text{O}$ values.

Based on detailed diagenetic analyses of the rock unit, it is assumed that Mg-rich fluids might have been supplied from the underlying siliciclastic Charun Quartzite or from the magmatic plutons during the thrusting of Devonian Shogram Formation over Cretaceous Reshun Formation (Fig. 1a) [12]. The thrusting occurred along the Northeast-Southwest Reshun Fault whereby migration pathways for the fluids have been generated. Consequently, various stages of dolomitization have been evolved in response to regeneration of fluids.

Dolomitization model

The Devonian Shogram Formation in the study area has undergone multiple episodes of deformation and plutonism (discussed earlier). The Shogram Formation is a burial dolomitization model based on stratigraphic and structural settings, field observations, petrography, and geochemistry (Fig. 6). In general, burial dolomitization models are essentially hydrological models. They differ mainly in the nature of the drives and direction of fluid flow [34]. The development of non-planar crystal textures at temperature higher than 60°C and the presence of saddle dolomite suggest the temperature of formation was higher than 80°C [35]. The initial phase of dolomitization (D1 and D2) resulted from the compaction flow of overlying Sarikol Shales which is evident by the low content Fe and Mn and less depleted $\delta^{18}\text{O}$ values at shallow depth [36]. Increasing burial resulted in the formation of D3 dolomite which was evident by more redox conditions met at depth and high depleted values of $\delta^{18}\text{O}$. Finally, activation of regional Reshun fault provided pathways for Mg-rich dolomitizing fluids from the deeper source resulting in the formation of D4 and SD as evident by more

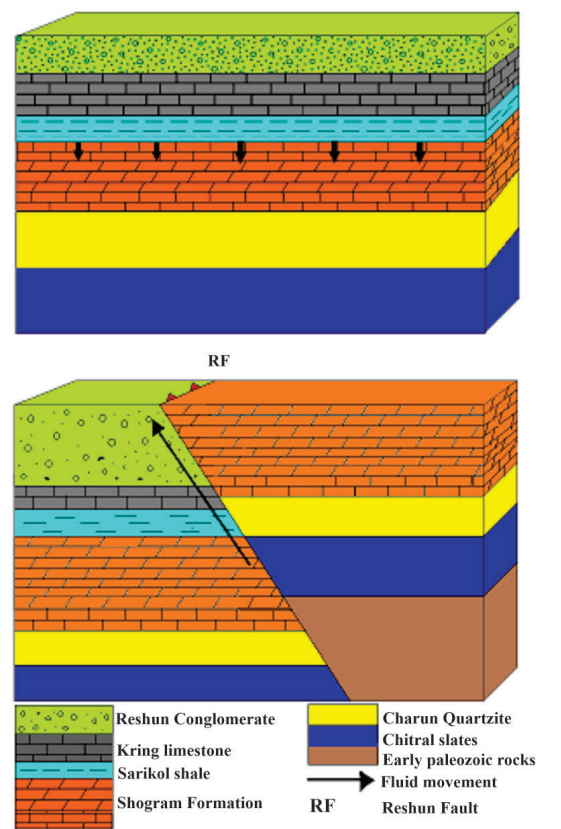


Fig. 6 Dolomitization model for the dolomites of Shogram Formation.

depleted values of $\delta^{18}\text{O}$ values and the presence of certain hydrothermal minerals in D4. The source of Mg-rich hydrothermal fluids in D4 could be widespread tectonic activity in Karakorum region during collisional or post-collisional times [7].

CONCLUSION

A detailed petrographic study of dolomites of Devonian Shogram Formation in Northwestern Karakorum revealed 4 types of replacive dolomites along with saddle dolomite. Fe and Mn contents in all dolomititic phase were high, specifically highest in D3 and D4, which shows reducing environment conditions. Sr content was higher in D1 while D4 was the lowest, indicating late diagenetic environment for the later phases of dolomite. For oxygen isotopic signature, D1 and D2 showed less depleted $\delta^{18}\text{O}$ values, whereas D3 and D4 had more depleted $\delta^{18}\text{O}$ isotope values, indicating multiphase dolomitization. Furthermore, saddle dolomite cement (SD) exhibited highly depleted $\delta^{18}\text{O}$ values. Conceptual dolomitization model suggested that multiphase dolomitization occurs in 3 phases. Initially, replacive dolomites (D1 and D2) are formed under compaction flow regime in shallow burial con-

ditions, which is supported by petrographical and geochemical data. It is followed by deep burial conditions which resulted in the formation of dolomite (D3), evident by more depleted $\delta^{18}\text{O}$ values and enhanced Fe and Mn contents. Moreover, dolomites (D4 and SD) are related with the activation of Northeast-Southwest Reshun fault, providing pathways for the Mg-rich hydrothermal fluids; this is supported by highly depleted $\delta^{18}\text{O}$ values, high Fe and Mn contents, and presence of high temperature hydrothermal minerals along with dolomite (D4). Possible source of hydrothermal fluids in later stages could be magmatic or deep-seated hydrothermal fluids which circulated along the faults

Appendix A. Supplementary data

Supplementary data associated with this article can be found at <http://dx.doi.org/10.2306/scienceasia1513-1874.2022.043>.

Acknowledgements: This work is the part of PhD dissertation of Maryam Saleem. The authors are thankful to Afsar Khan and Mustansir for their help and support during the field work.

REFERENCES

- Hardie LA (1987) Dolomitization: a critical view of some current views. *J Sediment Petrol* **57**, 166–183.
- Martín-Martín JD, Travé A, Gomez-Rivas E, Salas R, Sizun JP, Vergés J, Alfonso P (2015) Fault-controlled and stratabound dolostones in the Late Aptian–earliest Albian Benassal Formation (Maestrat Basin, E Spain): Petrology and geochemistry constrains. *Mar Pet Geol* **65**, 83–102.
- Muir-Wood R (1994) Earthquakes, strain-cycling and mobilization of fluids. *Geol Soc London, Spec Publ* **78**, 85–98.
- Hendry JP, Gregg JM, Shelton KL, Somerville ID, Crowley SF (2015) Origin, characteristics and distribution of fault-related and fracture-related dolomitization. *Contrib Sedimentol* **62**, 717–752.
- Lemennicier Y, Le Fort P, Lombardo B, Pêcher A, Rolfo F (1996) Tectonometamorphic evolution of the central Karakorum (Baltistan, northern Pakistan). *Tectonophysics* **260**, 119–143.
- Searle M (2011) Geological evolution of the Karakoram Ranges. *Int J Geosci* **130**, 147–159.
- Gaetani M, Mawson R, Sciunnach D, Talent JA (2008) The Devonian of Western Karakorum (Pakistan). *Acta Geol Pol* **58**, 261–285.
- Zanchi, Andrea, Gritti D (1996) Multistage structural evolution of Northern Karakorum (Hunza region, Pakistan). *Tectonophysics* **260**, 145–165.
- Hubmann B, Gaetani M (2007) Devonian calcareous algae, tabulate corals and bioclaustrations from the Karakorum mountains (northern Pakistan). *Riv Ital Ginecol* **113**, 307–328.
- Pudsey CJ, Coward MP, Luff IW, Shackleton RM, Windley BF, Jan MQ (1985) Collision zone between the Kohistan arc and the Asian plate in NW Pakistan. *Earth Environ Sci Trans R Soc Edinb* **76**, 463–479.
- Zanchi A, Poli S, Fumagalli P, Gaetani M (2000) Mantle exhumation along the Tirich Mir Fault Zone, NW Pakistan. *Geol Soc London, Spec Publ* **170**, 237–252.
- Zanchi A, Gaetani M, Poli S (1997) The Rich Gol Metamorphic complex: evidence of separation between Hindu Kush and Karakorum (Pakistan). *Proc Indian Acad Sci Earth Planet Sci* **325**, 877–882.
- Dickson JAD (1966) Carbonate identification and genesis as revealed by staining. *J Sediment Petrol* **36**, 491–505.
- Rosenbaum J, Sheppard SMF (1986) An isotopic study of siderites, dolomites and ankerites at high temperatures. *Geochim Cosmochim Acta* **50**, 1147–1150.
- Desio A, Martina E (1972) Geology of the upper Hunza valley, Karakorum, west Pakistan. *Boll Soc Geol Ital* **91**, 283–314.
- Sibley DF, Gregg JM (1987) Classification of dolomite rock textures. *J Sediment Res* **57**, 967–975.
- Veizer J (1983) Trace elements and isotopes in sedimentary carbonates. In: Reeder RJ (ed) *Carbonates: Mineralogy and Chemistry*, De Gruyter, Berlin, pp 265–300.
- Humphrey JD, Quinn TM (1989) Coastal mixing zone dolomite, and massive dolomitization of platform-margin carbonates. *J Sediment Petrol* **59**, 438–454.
- Qing H (1998) Petrography and geochemistry of early-stage, fine- and medium-crystalline dolomites in the Middle Devonian Presqu'île Barrier at Pine Point, Canada. *Evol Concepts Sedimentol Essays Conf* **45**, 433–446.
- Gaetani M (1997) The Karakorum block in central Asia, from Ordovician to Cretaceous. *Sediment Geol* **109**, 339–359.
- Kazmi AH, Jan MQ (1997) *Geology & Tectonics of Pakistan*, Graphic Publications.
- Dawans JM, Swart PK (1988) Textural and geochemical alternations in Late Cenozoic Bahamian dolomites. *Contrib Sedimentol* **35**, 385–403.
- Sibley DF, Gregg JM, Brown RG, Laudon PR (1993) Dolomite crystal size distribution. In: Rezak R, Lavoie DL (eds) *Carbonate Microfabrics*, Frontiers in Sedimentary Geology, Springer, New York, NY, pp 195–204.
- Duggan JP, Mountjoy EW, Stasiuk LD (2001) Fault-controlled dolomitization at Swan Hills Simonette oil field (Devonian). *Dev Sedimentol* **48**, 301–323.
- Hou MC, Jiang WJ, Xing FC, Xu SL, Liu XC, Xiao C (2016) Origin of dolomites in the Cambrian (upper 3rd-Furongian) formation, south-eastern Sichuan Basin, China. *Geofluids* **16**, 856–876.
- Machel HG (2004) Concepts and models of dolomitization: A critical reappraisal. *Geol Soc London, Spec Publ* **235**, 7–63.
- Warren J (2000) Dolomite: Occurrence, evolution and economically important associations. *Earth Sci Rev* **52**, 1–81.
- Kouchinsky A, Bengtson S, Gallet Y, Korovnikov I, Pavlov V, Runnegar B, Shields G, Veizer J (2008) The SPICE carbon isotope excursion in Siberia. *Geol Mag* **145**, 609–622.
- Huang SJ, Shi H, Mao XD, Zhang M, Shen LC, Wu W-H (2003) Diagenetic alteration of earlier Paleozoic marine carbonate and preservation for the information of sea water. *J Chengdu Univ Sci Technol* **30**, 9–18.
- Machel HG, Anderson JH (1989) Pervasive subsurface dolomitization of the Nisku formation in central Alberta. *J Sediment Res* **59**, 891–911.

31. Banner JL, Hanson GN, Meyers WJ (1988) Water-rock interaction history of regionally extensive dolomites of the Burlington-Keokuk formation (Mississippian). *Soc Econ Paleont Min, Spec Publ* **43**, 97–113.
32. Zheng X, Arps PJ, Smith RW (1999) Adsorption of *Bacillus subtilis* to minerals. *Miner Process Extr Metall Rev* **9**, 127–136.
33. Lorens RB (1981) Sr, Cd, Mn and Co distribution coefficients in calcite as a function of calcite precipitation rate. *Geochim Cosmochim Acta* **45**, 553–561.
34. Morrow DW (1982) Diagenesis 2. Dolomite: Part 2. Dolomitization models and ancient dolostones. *Proc Geol Assoc Can* **9**, 95–107.
35. Spötl C, Pitman JK (1998) Saddle (baroque) dolomite in carbonates and sandstones: a reappraisal of a burial-diagenetic concept. Carbonate Cementation in Sandstones. *Int Assoc Sedimento, Spec Publ* **26**, 437–460.
36. Koeshidayatullah A, Corlett H, Stacey J, Swart PK, Boyce A, Robertson H, Whitaker F, Hollis C (2020) Evaluating new fault-controlled hydrothermal dolomitization models: Insights from the Cambrian Dolomite, Western Canadian Sedimentary Basin. *Sedimentology* **67**, 2945–2973.

Appendix A. Supplementary data

Table S1 Elemental analyses of the different dolomite phases.

Sample no.	Stage	Fe (ppm)	Mn (ppm)	Sr (ppm)	Na (ppm)
SMS-05	D1	4251.62	386	174	290
SMS-09	D1	4260.84	394	137	287
SMS-26-A	D1	5245.32	372	188	295
SMS-27	D1	5260.71	393	144	250
SMS-35	D1	4961.64	436	131	241
SMS-41-B	D1	5943.74	475	153	236
SMS-46	D1	5972.28	479	174	247
SMS-49	D1	4609.05	397	143	276
SMS-51	D1	4035.94	388	167	231
SMS-55-A	D1	4027.48	396	160	284
SMS-59	D1	4961.65	391	145	261
SMS-60	D1	5488.73	380	144	243
SMS-75-A	D2	6402.35	445	120	169
SMS-82	D2	7158.02	472	118	157
SMS-87	D2	7265.75	435	107	160
SMS-93	D2	7951.32	385	99	132
SMS-102	D2	7968.25	372	77	154
SMS-113-A	D2	8084.25	489	120	127
SMS-128	D2	8263.51	466	131	139
SMS-136	D2	8532.25	492	101	155
SMS-151	D2	8598.37	435	114	146
SMS-173	D2	8932.25	487	76	115
SMS-189	D2	8914.12	427	109	124
SMS-207-B	D2	8830.54	476	127	164
SMS-218	D2	8957.68	445	104	140
SMS-251	D3	8302.32	385	103	105
SMS-284-B	D3	8189.17	456	105	99
SMS-292	D3	8469.53	376	76	84
SMS-315	D3	8968.43	521	90	108
SMS-328	D3	9821.62	490	71	135
SMS-351	D3	9906.34	548	78	119
SMS-364	D3	9467.81	481	89	89
SMS-377	D3	9397.35	492	73	84
SMS-381	D3	9674.67	512	81	119
SMS-392	D3	9979.76	485	77	121
SMS-409	D4	9580.15	485	113	84
SMS-418-A	D4	9586.41	478	84	67
SMS-438-A	D4	10067.32	452	119	101
SMS-442-B	D4	10564.37	425	116	57
SMS-462	D4	10494.26	584	120	43
SMS-487	D4	10047.99	554	78	51

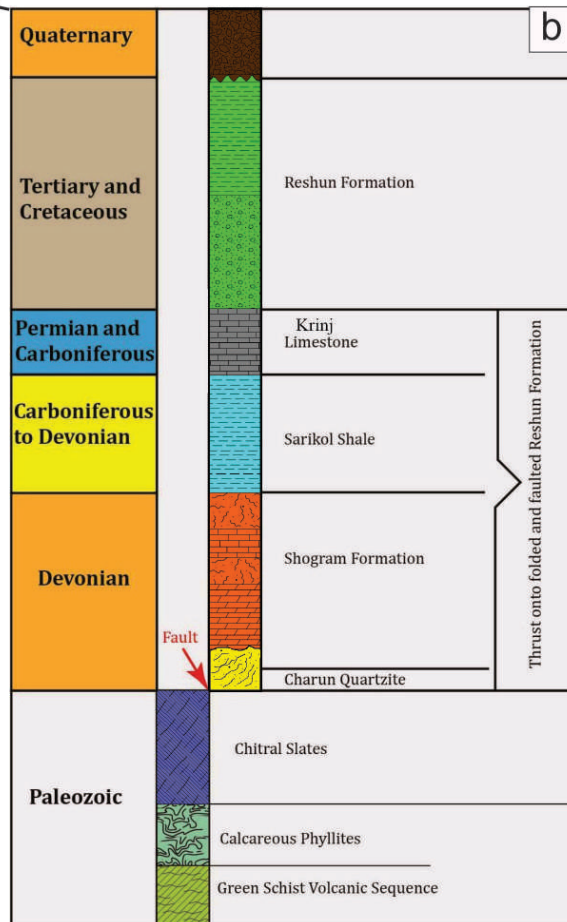
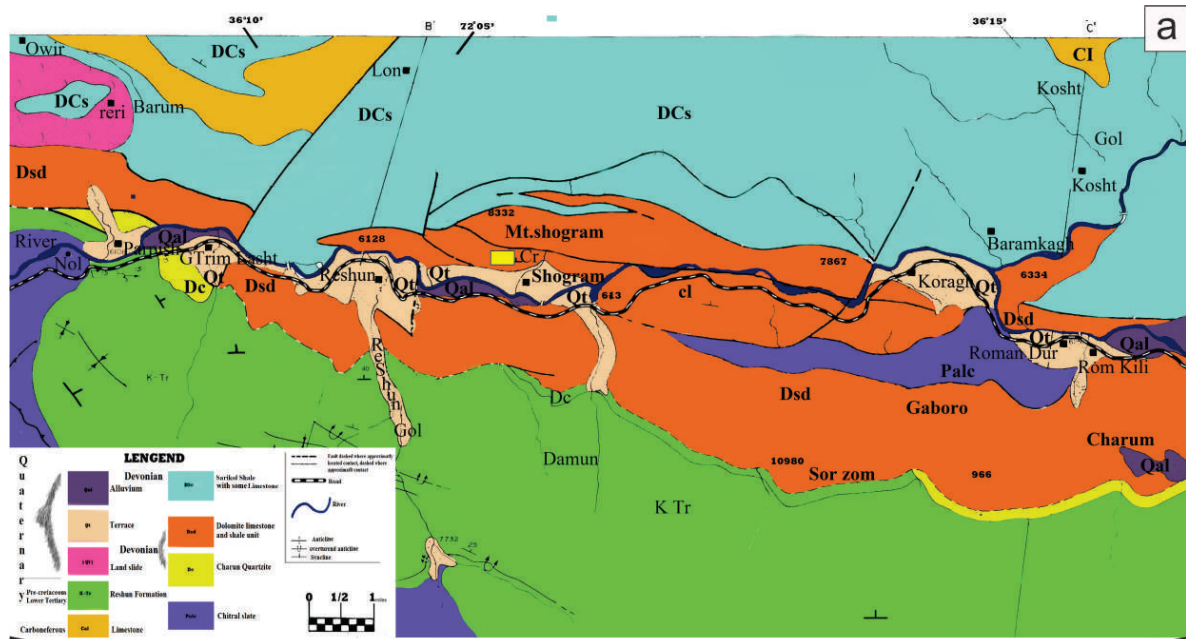


Fig. S1 (a) Geological map of Western Karakoram where the yellow box shows the location of study area. (b) Stratigraphic log of the study area.